ACS OMEGA

http://pubs.acs.org/journal/acsodf

Article

$NiCo_2S_4$ Bi-metal Sulfide Coating on $LiNi_{0.6}Co_{0.2}Mn_{0.2}O_2$ Cathode for High-Performance All-Solid-State Lithium Batteries

Young-Jin Kim, Rajesh Rajagopal, Sung Kang, and Kwang-Sun Ryu*

Cite This: *ACS Omega* 2021, 6, 6824−6835

Read Online

ACCESS | Metrics & More | Article Recommendations

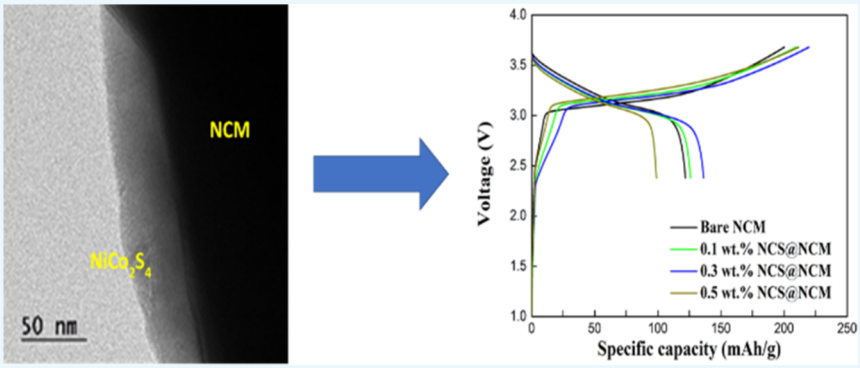

ABSTRACT: $NiCo_2S_4$ nanoparticles (NPs) were dry coated on $LiNi_{0.6}Co_{0.2}Mn_{0.2}O_2$ (NCM622) cathode using a resonant acoustic coating technique to produce all-solid-state lithium batteries. The $NiCo_2S_4$ coating improved the electrochemical properties of the NCM622 cathode. In addition, $NiCo_2S_4$ eliminated the space-charge layer and the cathode showed an excellent affinity with the interface with a sulfide-based solid electrolyte as an inert material. X-ray diffraction patterns of NCM622 coated with $NiCo_2S_4$ showed the same peak separations and lattice parameters as those of bare NCM622. Field-emission scanning electron microscopy and electron dispersive spectroscopy mapping analyses showed that 0.3 wt% $NiCo_2S_4$-coated NCM622 had an evenly modified surface with $NiCo_2S_4$ NPs. X-ray photoelectron spectroscopy (XPS) revealed that the surface of 0.3 wt% $NiCo_2S_4$-coated NCM622 had two different S 2p peaks, a Co−S peak, and Ni and Co peaks, compared to those of bare NCM622. Electrochemical studies with electrochemical impedance spectroscopy and galvanostatic charge−discharge cycle performances showed that $NiCo_2S_4$-coated NCM622 retained a higher specific capacity over multiple cycles than bare NCM622. Especially, 0.3 wt% $NiCo_2S_4$-coated NCM622 exhibited a capacity retention of 60.6% at a current density of 15 mA/g for 20 cycles, compared to only 37.3% for bare NCM622. Finally, interfacial XPS and transmission electron microscopy-electron energy loss spectroscopy analyses confirmed the stable state of 0.3 wt% $NiCo_2S_4$-coated NCM622 with minimal side reactions.

1. INTRODUCTION

Nowadays, lithium-ion batteries have been applied as energy storage systems for large-scale batteries and electric vehicles because of their high energy density and power density. On the other hand, lithium-ion batteries have critical problems because of their use of flammable organic electrolytes. Because of uncertainties in safety problems in energy storage systems, the commercialization of lithium-ion batteries remains in doubt.[1−3]

All-solid-state lithium batteries (ASSLBs) are one of the most promising next-generation batteries as a potential game changer since they can realize high-energy density with added safety. In addition, much research has focused on oxide, sulfide, and polymer-based solid electrolytes by applying ASSLBs. In particular, sulfide-based solid electrolytes have the highest conductivity of lithium ions. Because of their soft properties, they are easily used as solid electrolytes. Usually, solid electrolytes have a wide electrochemical window of up to 5 V, which can be used to commercialize a high-density energy storage system. Thus, many sulfide-based solid electrolytes have ionic conductivities ranging from 10^{-5} to 10^{-3} S/cm. Kanno et al. have presented a lithium superionic conductor with an ionic conductivity of 10^{-2} S/cm ($Li_{10}GeP_2S_{12}$).[4,5]

A variety of cathode materials, including $LiNi_xCo_yMn_zO_2$ (NCM), $LiCoO_2$ (LCO), $LiNi_xCo_yAl_zO_2$ (NCA), and $LiFePO_4$, have been used for ASSLB applications. Among them,

Received: December 6, 2020
Accepted: February 12, 2021
Published: March 8, 2021

NCM and LCO have received much attention because of their high theoretical capacity and compatibility against inorganic solid electrolytes.[6−9] Unfortunately, high interfacial resistance lowers the lithium ion conductivity compared to that of organic electrolytes, thus degrading the capacity.[10−12] These cathode interfaces have been coated with various oxides, including $LiNbO_3$, $LiAlO_2$, or Li_2ZrO_3, to protect the interface or to relieve side reactions. Many studies have tried to impose conditions that do not prevent the entry of lithium ions when the buffer layer is formed. However, very few sulfide-coating studies have taken account of the physical properties of sulfide-based solid electrolytes.[13−16]

Sakuda et al. have studied cobalt sulfide-coated $LiCoO_2$ and nickel sulfide-coated $LiCoO_2$ by using sol−gel method followed by thermal decomposition technique and reported higher initial specific capacity. Subsequently, however, no study has reported a better cycle maintaining rate. No further sulfide coating studies with the cathode surface in ASSLBs have been conducted since the last few years.[17] The CoS coating can increase the electrochemical behavior of the cathode material like a semiconductor (~0.5−1.5 eV). On the other hand, the cathode electrode's active material of cobalt is not expected to play a role other than preventing direct contact with the interface. Interestingly, bi-metal sulfides solve the above problems because of their higher electrochemical process. Usually, bi-metal sulfides have higher conductivity and are richer in active sites for redox reactions. These advantages are highly favorable for using the bi-metal sulfides as a cathode-coating material. In addition, electronegative sulfur atoms provide more space for lithium ion transport. Specifically, nickel-cobalt sulfide exhibits high theoretical capacity, long cycling stability, and strong redox reactions because of its variable oxidation states. However, nickel cobalt sulfide ($NiCo_2S_4$) is a stable supercapacitor material that does not consume lithium ions as a side reaction but holds them chemically. Thus, it has been used as a hybrid anode material. These findings allow sufficient interaction with the active material of the positive electrode to suppress the side reactions and maximize the electrochemical specific capacity of the electrode.

Therefore, we prepared bimetal sulfide ($NiCo_2S_4$) for use as a coating agent and lithium-scavenger material. $NiCo_2S_4$ was synthesized at the nanoparticle (NP) scale. The Ni-rich cathode was modified with this coating agent via a coating process that minimized the side reaction between the solid electrolyte and the cathode, thereby reducing the interfacial resistance of ASSLBs. Usually, $NiCo_2S_4$ NPs are selected for use as the anode or supercapacitor with an available Li^+ ion storage system.[18,19] Fortunately, our research produced satisfactory results, which will be useful for the continuous application of ASSLBs through new coating agents. In this work, we studied the coating effect of $NiCo_2S_4$ coating at the interface between the $LiNi_{0.6}Co_{0.2}Mn_{0.2}O_2$ (NCM622) and $Li_7P_2S_8I$ solid electrolyte.

2. EXPERIMENTAL SECTION

First, 0.39 g of $Co(NO_3)\cdot 6H_2O$ (Sigma-Aldrich, 98%), 0.193 g of $Co(NO_3)\cdot 6H_2O$ (Sigma-Aldrich, 99%), and 0.605 g of thiourea were dissolved in 40 mL of ethanolamine solvent (Samchun Chem., 99%) with triple-distilled water and stirred vigorously for 20 min to disperse every particle. Then, the solution was transferred to a 70 mL Teflon-lined stainless steel autoclave (ILSHIN AUTOCLAVE Inc., bolt closure pressure vessel) for solvothermal reaction at 200 °C for 14 h. After synthesis, the resultant product was collected and washed with distilled water and ethanol several times and dried at 60 °C overnight in a vacuum oven to make $NiCo_2S_4$ NPs.[18,19]

The synthesized $NiCo_2S_4$ NPs and NCM622 (obtained from a company in South Korea) cathode material were mixed homogeneously (0.1 wt% of $NiCo_2S_4$ by NCM weight and 10 g of NCM622 cathode) using a Thinky mixer, and the mixture was transferred into a specially designed zirconia container (fill up to 80%) and vibrated with a Resonant Acoustic Mixer (LabRAM II, Resodyn Inc.) at the vibration energy until 60 G for 20 min.[20−24] The $NiCo_2S_4$ clusters were continuously broken under shock or force to disperse $NiCo_2S_4$ NPs that homogeneously crashed into the surface of NCM622, which was coated with $NiCo_2S_4$ under conditions of 60 G with gravity acceleration for 20 min. Before setting this vibration energy and coating time, the parameters were optimized to obtain a proper coating without any damage. Using the same procedure, 0.3 and 0.5 wt% $NiCo_2S_4$-coated NCM622 samples were prepared.

Powder X-ray diffraction (XRD) measurements were conducted using XRD, Rigaku Ultima 4 with Cu Kα radiation (λ = 1.5418 Å) and a voltage of 40 kV and a current of 30 mA, and coupled with X'pert Highscore Plus software. $NiCo_2S_4$ NPs were first measured with 2θ = 10−90° at a step size of 0.02°. In addition, the metal sulfide-coated NCM622 samples were measured to determine whether the lattice of NCM622 was changed after the modification. The surface of NCM622 was measured using field-emission scanning electron microscopy (FE-SEM, JEOL, JSM-7610F) with energy dispersive X-ray spectroscopy (EDS, Oxford Instruments/x-MaxN). Before FE-SEM analysis, the carbon tape was attached to the copper mount substrate and the sample was spread over the carbon tape. Then, the sample was sputter coated with platinum for 30 s with an applied current of 30 mA to reduce the charging effects during the FE-SEM analysis, which was carried out at an operating voltage of 10 kV and a distance of 8 mm between the lens and sample. During the EDS analysis, the aperture voltage changed to 15 kV and the distance between the lens and sample was 8 mm. Field-emission transmission electron microscopy (FE-TEM, JEOL, JEM-2100F) with an accelerating potential of 200 kV was used to elucidate the surface of the $NiCo_2S_4$-coated NCM622 cathode material, including the coating thickness of the coating agent with the lattice parameter of NCM622 or metal sulfide. To optimize the results, the sample was dispersed on ethanol and sonicated. Then, the solution was added dropwise over the 200-mesh sized carbon-coated copper grid and dried. In addition, selected area diffraction was also performed to measure the lattice plane of the sample. The surface bonding structures of $NiCo_2S_4$-coated NCM622 was studied by X-ray photoelectron spectroscopy (XPS; ESCALAB250/VGScientific) with non-monochromatic Al Kα X-ray radiation ($h\nu$ = 1486.8 eV) as the excitation source and a pass (resolution) energy of 50 eV for wide scan (1 eV s^{-1}) and 20 eV for narrow scan (0.1 eV s^{-1}). XPS analysis was performed over the binding energy range of 0−1400 eV with a step size of 1 eV s^{-1}. Prior to the analysis, the sample was spread on a double-sided Cu sticky tape that was attached horizontally to the holder and placed normal to the electrostatic lens. XPS analysis was carried out at an applied voltage of 15 kV and a current of 10 mA. The analysis spot size of the powder sample was 500 μm, under large area XL lens mode and using the CAE: Pass Energy 50.0 eV

https://dx.doi.org/10.1021/acsomega.0c05942
ACS Omega 2021, 6, 6824−6835

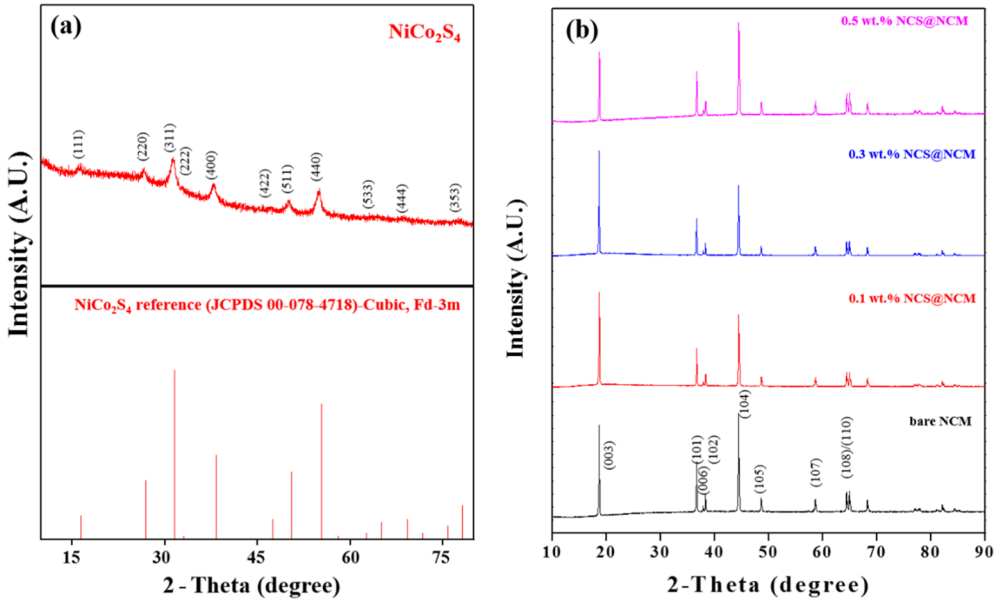

Figure 1. XRD patterns of (a) $NiCo_2S_4$ NPs and (b) bare NCM622 and $NiCo_2S_4$-coated NCM622 cathode materials.

analyzer mode. During the XPS analysis, charge neutralization was employed. The XPSPEAKS (V.4) software was used for fitting with Shirley background subtraction. In order to obtain the best fitting, Gaussian (Y %)−Lorentzian (X %) parameters were adjusted to obtain the desired line shapes and line widths.

For lab-scale active materials for ASSLBs, we prepared the cathode composite by mixing the $NiCo_2S_4$-coated NCM622 cathode, $Li_7P_2S_8I$ (1.28×10^{-3} S/cm) solid electrolyte, and super-P at a ratio of 70:28:2.[25−28] This mixture was pressed at 300 bars, followed by mixing with mortar and pestle. The above process was repeated three times to make homogeneous composites. To prepare a solid electrolyte pellet, 0.2 g of the $Li_7P_2S_8I$ was compressed at 300 bars for 5 min using a 16 mm mold. Then, 0.0200 g of the cathode composite was spread and compressed on one side of the solid electrolyte and a 50 μm-thick indium (In) foil (Nilaco) was attached to both sides and used as the current collector and anode material (anode side). Thin In foil is highly stable against sulfide-based solid electrolytes, but In foil (element) has a plateau of 0.62 V (vs Li/Li^+).[25−28]

The ASSLBs of $In|Li_7P_2S_8I|LiNi_{0.6}Co_{0.2}Mn_{0.2}O_2$ were assembled as a 2032 type coin-cell and subjected to electrochemical impedance spectroscopy (EIS) analysis using a SP-300 (BioLogic) analyzer at a frequency range of 1 MHz to 1 Hz to measure the internal resistance of the battery before and after the charge−discharge experiment. Charge and discharge cycle measurements were done within a voltage window from 3.68 to 2.38 V (WonATech electrochemical cycle system). The charge−discharge cycle performances were studied up to 20 cycles at an applied current density of 15 mA/g (0.1 C-rate) and at room temperature (25 °C). In addition, the C-rate performances were studied from 0.05 C-rate (7.5 mA/g) to 2 C-rate (300 mA/g). The galvanostatic intermittent titration technique (GITT) was used to analyze the Li^+ ion diffusion characteristics after 20 cycles with a pulse current of 0.1 C (5 μA/10 μA) intermittently for 10 min. The contact area between the NCM material and sulfide-based solid electrolyte particles was obtained by GITT measurements using the following equation.[29]

$$D_{Li^+} = \frac{4}{\pi\tau}\left(\frac{m_B V_M}{M_B A}\right)^2\left(\frac{\Delta E_S}{\Delta E_\tau}\right)^2$$

D: ion-diffusion coefficient of NCM, ΔE_τ: transient voltage change, A: contact area between the sulfide-based solid electrolyte and cathode materials, τ: pulse duration (10 min), ΔE_S: steady-state voltage change, M_B: molecular weight of the $Ni_{0.6}Co_{0.2}Mn_{0.2}O_2$ (90.13 g/mol), M_{ncm}: mass of the host in the sample (varied depending on the mass loading sample), and V_m: molar volume of the material (the value used was for $LiNi_{1/3}Co_{1/3}Mn_{1/3}O_2$, 20.29 cm^3/mol).[29]

The chemical diffusion coefficient (D) value of NCM of 1.72×10^{-11} cm^2/s was obtained from GITT references using an NCM622/Li cell with an organic electrolyte.[29]

We prepared the interfacial area between the NCM622 cathode and the $Li_7P_2S_8I$ electrolyte (0.3 wt $NiCo_2S_4$-coated NCM622/$Li_7P_2S_8I$/super P composite) using focused ion beam equipment (Quanta 3D FEG, FEI) for cutting micro-sized samples. We analyzed the degree of TEM−electron energy loss spectroscopy (EELS) precision (Titan 80-300) with EELS (installed in the TEM). XPS (Thermo Scientific, ESCALAB 250) measurements of the cathode composite after 20 cycles were additionally analyzed to study the side reactions on the cathode composites/$Li_7P_2S_8I$ solid electrolyte interface. Before this analysis, the electrode composite of ASSLBs (after 20 cycles) was separated from the cell and spacer. This electrode material was sealed in vacuum and transferred to the instrument. The top surface (~50 nm) was raked to gather the cathode parts. The cross-sectional interface was prepared using an FIB-TEM grid with vacuum transfer equipment. Then, we carefully observed the interface area between the coated cathode material and the solid electrolyte.[3]

3. RESULTS AND DISCUSSION

Figure 1a shows the powder XRD patterns of the $NiCo_2S_4$ NPs only with the reference pattern to confirm whether it was synthesized or not. After synthesis of each single substance of the metal sulfide, the XRD patterns of bare NCM622 and $NiCo_2S_4$-coated NCM622 (0.1, 0.3, and 0.5 wt % by mass ratio

https://dx.doi.org/10.1021/acsomega.0c05942
ACS Omega 2021, 6, 6824−6835

Table 1. Lattice Parameters of Bare NCM622 and $NiCo_2S_4$-Coated NCM622 Cathode Materials Coated with Different Amounts of Coating Agents

material	calculated lattice parameter (Å)		
	A	*C*	*c*/*a* ratio
bare NCM622	2.870	14.25	4.965
0.1 wt % $NiCo_2S_4$ @ NCM	2.872	14.23	4.955
0.3 wt % $NiCo_2S_4$ @ NCM	2.869	14.24	4.963
0.5 wt % $NiCo_2S_4$ @ NCM	2.868	14.23	4.962

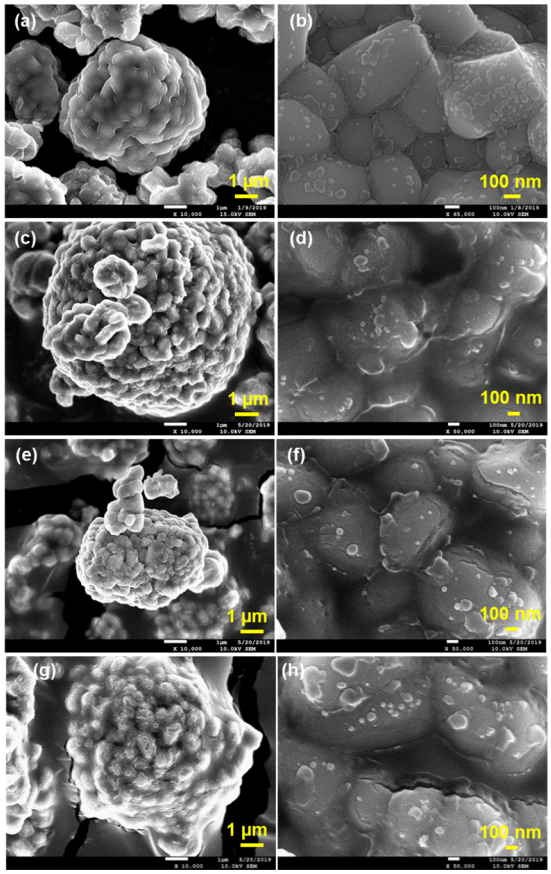

Figure 2. FE-SEM images of (a,b) bare NCM622, (c,d) 0.1, (e,f) 0.3, and (g,h) 0.5 wt % $NiCo_2S_4$-coated NCM622 with different magnifications.

of NCM622) were obtained, and the results are shown in Figure 1b. As shown in Figure 1a, synthesized $NiCo_2S_4$ NPs exhibited a cubic structure (JCPDS 00-075-2157) with $Fd\bar{3}m$ space group.[14,19] As shown in Figure 1b, the XRD diffraction patterns of the NCM622 composites match with the layered hexagonal alpha-$NaFeO_2$ crystal structure ($R\bar{3}m$ space groups). The lattice parameters of all samples were calculated using the X'Pert software, and the values are shown in Table 1.[30,31] No significant changes were observed in the surface-modified NCM622. The diffraction peaks for $NiCo_2O_4$ NPs were seldom detected in all samples. This indicates that only a small amount of $NiCo_2O_4$ NPs may coat over the surface of NCM622 cathode materials.

FE-SEM images (Figure 2a–h) show the $NiCo_2S_4$-coated NCM samples. An EDS image of 0.3 wt% $NiCo_2S_4$-coated NCM622 and pure $NiCo_2S_4$ NPs with S, O, Ni, Co, and Mn elements are shown in Figure 3a–c. The morphology of the $NiCo_2S_4$ NP cluster is shown in Figure 3a,b. The morphologies

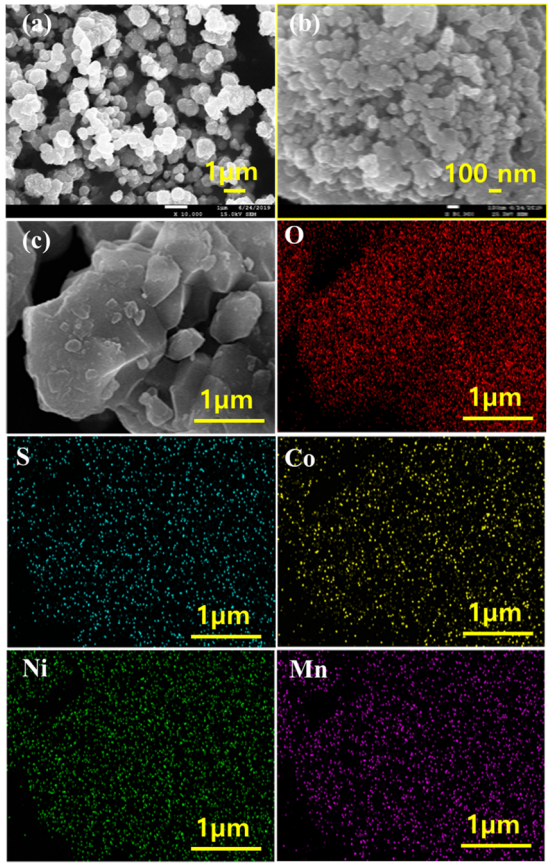

Figure 3. FE-SEM images of (a,b) $NiCo_2S_4$ NP at different magnification, (c) selected area of 0.3 wt % $NiCo_2S_4$-coated with O, S, Co, Ni, and Mn elements.

of the bare NCM622 and $NiCo_2S_4$-coated NCM622 cathode materials are shown in Figure 2a–h. The surface of the bare NCM was clear, while 0.1 and 0.3 wt% $NiCo_2S_4$-coated NCM622 (Figure 2c–f) show uniformly distributed $NiCo_2S_4$ NPs, and 0.3 wt % $NiCo_2S_4$-coated NCM622 shows denser NPs than 0.1 wt% $NiCo_2S_4$-coated NCM622, indicating that the direct coating with the resonant acoustic technique was successful. Further increasing the NP concentration to 0.5 wt% (Figure 2g,h) produced a thicker and denser coating. This nickel cobalt sulfide NP modification may have decreased the interfacial resistance, although it may also have obstructed the lithium ion transfer pathway. Therefore, reducing the nanomaterial size to approximately 10 nm may further improve the surface-modified NPs and their physical or electrochemical qualities.

Figure 4a,b shows the FE-TEM images of $NiCo_2S_4$ NPs with a *d*-space length of $NiCo_2S_4$. The size of $NiCo_2S_4$ ranged from 10 to 50 nm. The $NiCo_2S_4$ NPs have cubic (311) and (111) planes with lattice lengths of 0.279 and 0.538 nm, respectively.[17,18] Figure 4c,d displays the FE-TEM images of $NiCo_2S_4$-coated NCM622 with *d*-space length. The size of $NiCo_2S_4$ NPs was measured as ranging from 10 to 50 nm. The $NiCo_2S_4$ NPs of 0.3 wt% $NiCo_2S_4$-coated NCM622 showed only a single lattice of cubic crystalline of (311) plane with a lattice length of 0.279 nm with a $NiCo_2S_4$ thickness of less than 40 nm.

XPS examination of 0.3 wt % $NiCo_2S_4$-coated NCM622 was conducted to analyze the chemical binding energy of the NCM622 cathode material modified with metal sulfide. All the

https://dx.doi.org/10.1021/acsomega.0c05942
ACS Omega 2021, 6, 6824–6835

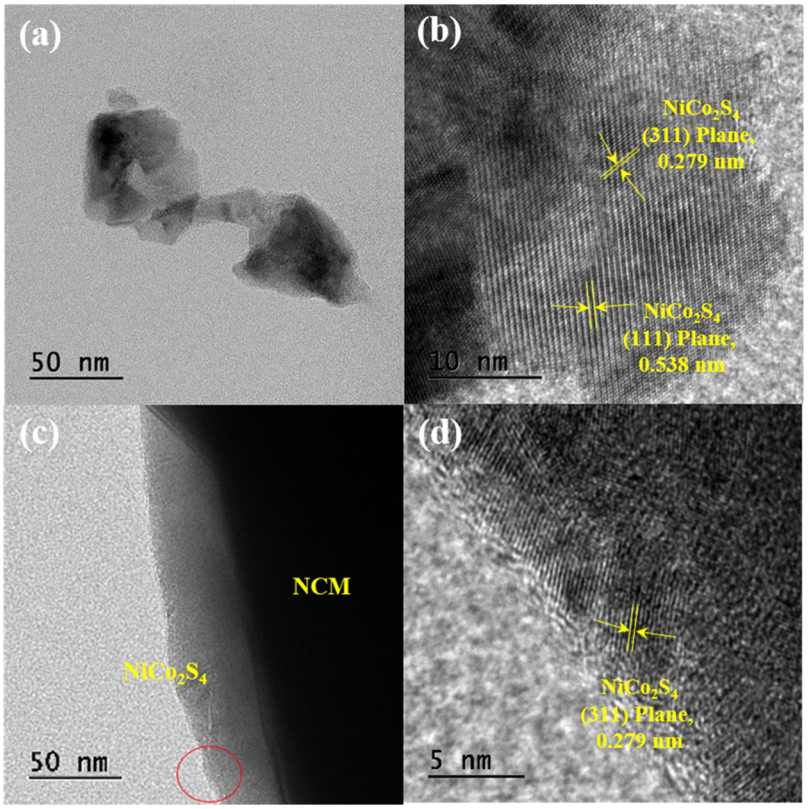

Figure 4. FE-TEM images of (a) NP of $NiCo_2S_4$, (b) lattice length of $NiCo_2S_4$, and (c,d) 0.3 wt% $NiCo_2S_4$-coated NCM622.

XPS spectra are shown in Figure 5. The survey scan from 0 to 1300 eV is shown in Figure 5a. The XPS spectrum of $NiCo_2S_4$-coated NCM622 revealed peaks for Ni $2p_{3/2}$ (entirely 855.5 from +3 charge and 854.5 eV from +2 charge) and Ni $2p_{1/2}$ (873.2 eV), with the addition of two satellite peaks at 861.2 and 879.5 eV (Figure 5b).[30,31] The Ni $2p_{3/2}$ scan showed the oxidation state of Ni^{2+} (854.5 eV) and Ni^{3+} (855.5 eV). The satellite peaks from Ni $2p_{3/2}$ and Ni $2p_{1/2}$ were detected strongly at 861.1 and 879.4 eV, respectively, which were attributed to the NCM622 cathode. On the other hand, a peak for Ni $2p_{3/2}$ of Ni−S was weakly detected because of the $NiCo_2S_4$ NP modification.

As shown in Figure 5c, the peaks at 780.5 and 764.2 eV correspond to Co $2p_{3/2}$ and Co $2p_{1/2}$, respectively. A weak satellite peak was detected at 787.0 eV with the oxidation state of 3^+ charge. Another Co $2p_{3/2}$ peak of Co−S is shown at 783.8, indicating that $NiCo_2S_4$ NPs could be detected easily, as reported previously.[17,18] Figure 5d shows S 2p peaks of $NiCo_2S_4$-coated NCM622. Two S 2p peaks of 0.3 wt% $NiCo_2S_4$-coated NCM622 were detected at 162.0 and 168.7 eV because the bimetal sulfide has more complicated metal-S peaks, while the Ni−S peak has a weaker binding energy than Co−S. As a result, we were able to chemically prove that NCM622 coated with $NiCo_2S_4$ NPs had a different chemical binding energy than that of the single metal sulfide.

Figure 6a,b shows the galvanostatic initial charge−discharge behaviors of the $In|Li_7P_2S_8I|LiNi_{0.6}Co_{0.2}Mn_{0.2}O_2$ ASSLB system using bare NCM622, and 0.1, 0.3, and 0.5 wt% $NiCo_2S_4$-coated NCM622 cathode materials at the current densities of 15 mA/g (0.1 C-rate) and 7.5 mA/g (0.05 C-rate). The charge−discharge analysis was performed between the potentials of 3.68 and 2.38 V at room temperature (25 °C). The calculated discharge capacities of all cathode materials are listed in Table 2. The first discharge capacity of bare NCM622 was 86.0 mA h/g at 15 mA/g and 121.82 mA h/g at 7.5 mA/g. The calculated specific capacities of 0.1, 0.3, and 0.5 wt% $NiCo_2S_4$-coated NCM622 were 115.9, 118.0, and 84.7 mA h/g, respectively, at a current density of 15 mA/g. This trend of increasing discharge capacity revealed that the interfacial resistance or contact loss was relieved by coating with 0.1 and 0.3 wt% $NiCo_2S_4$ NPs. However, 0.5 wt % $NiCo_2S_4$-coated NCM622 had a specific capacity of only 84.5 mA h/g, which is lower than bare NCM622, indicating that $NiCo_2S_4$ NPs coating at high concentration does not provide a satisfactory coating effect because an excessive number of $NiCo_2S_4$ NPs fail to attach to the cathode and instead form as separate NPs. The NCM622 cathode coated with $NiCo_2S_4$ NPs exhibited a discharge capacity value of 121.82 mA/g at low current density of 7.5 mA/g. As shown in Figure 6b, the specific capacities of 0.1, 0.3, and 0.5 wt% $NiCo_2S_4$-coated NCM622 samples were 125.97, 128.7, and 98.9 mA h/g, respectively, at a current density of 7.5 mA/g. This indicates that the $NiCo_2S_4$ NPs can catch or retain the lithium ion without consuming any inert material or scavenger generated by the side reaction which maintained the high capacity.

After the initial charge−discharge analysis, we studied the cycle performances with c-rate performances. Figure 7a shows the charge−discharge cycle performances of the bare NCM622 and $NiCo_2S_4$-coated NCM622 cathode composites at a current density of 15 mA/g for 20 cycles, and the results are shown in Figure 7b. Of the cells using the $NiCo_2S_4$-coated NCM622 cathode materials, 0.1 and 0.3 wt% $NiCo_2S_4$-coated NCM622 had higher initial capacities (115.9 and 118.0 mA h/g, respectively) than that of 0.5 wt% $NiCo_2S_4$-coated NCM622. On the other hand, the cycle stability performance of 0.1 wt% $NiCo_2S_4$-coated NCM622 was worse than that of 0.5 wt%

https://dx.doi.org/10.1021/acsomega.0c05942
ACS Omega 2021, 6, 6824−6835

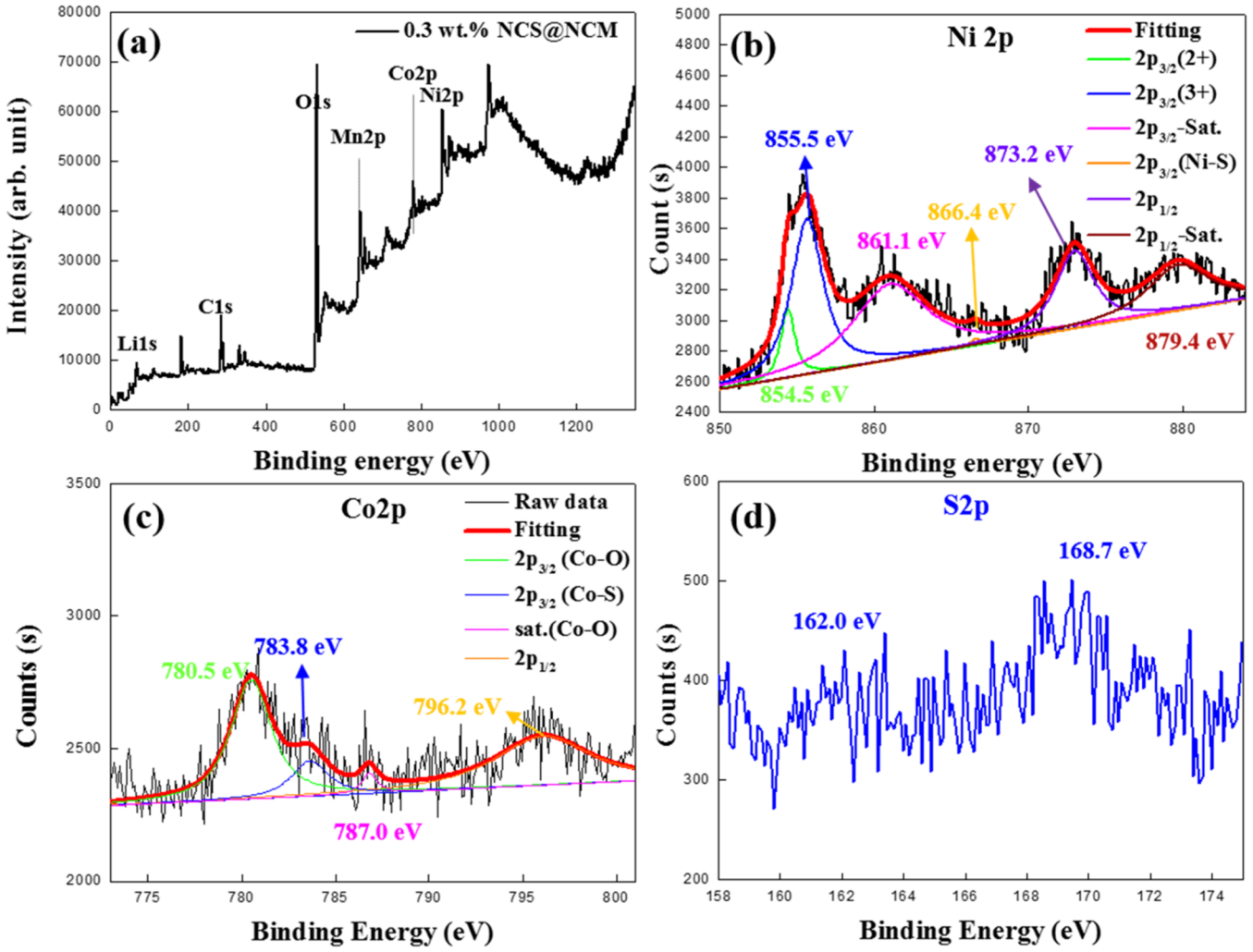

Figure 5. XPS graphs of (a) survey spectrum, (b) Ni 2p, (c) Co 2p, and (d) S 2p of 0.3 wt% $NiCo_2S_4$-coated NCM622.

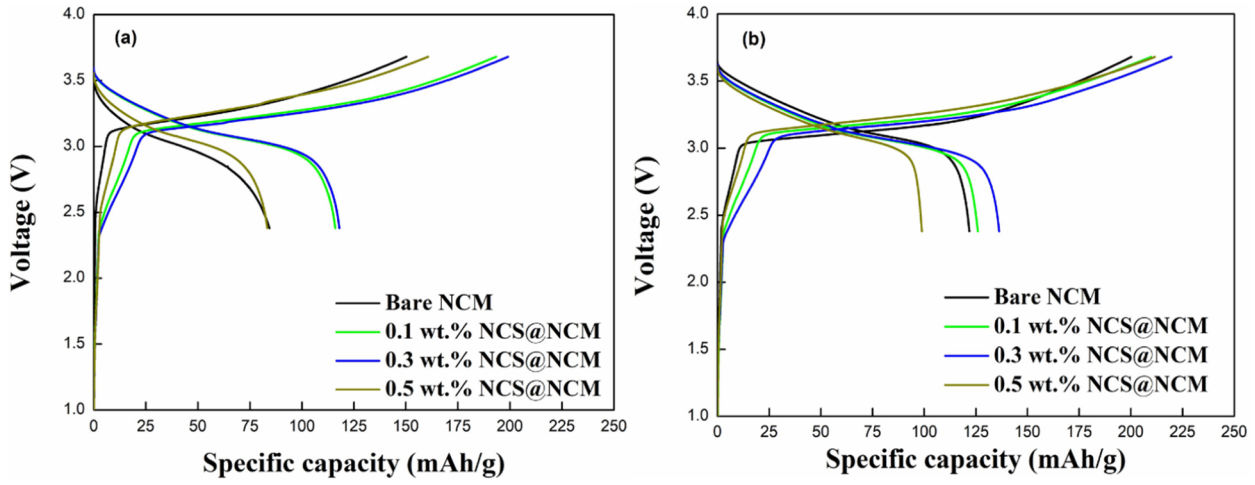

Figure 6. Charge and discharge curves of (a) 0.1 c-rate (15 mA/g) and (b) 0.05 c-rate (7.5 mA/g) using the $In|Li_7P_2S_8I|LiNi_{0.6}Co_{0.2}Mn_{0.2}O_2$ cell.

$NiCo_2S_4$-coated NCM622. The calculated specific capacity retention of the 0.1 and 0.3 wt% $NiCo_2S_4$-coated NCM622 cathode composites was 44.6 and 60.6%, respectively.

However, the capacity retention rates were much higher than those of the other compositions. Among all the samples, the highest capacity retention rate was 76.6%. Figure 7c shows the calculated discharge capacities according to the C-rate performance at the applied current densities of 7.5, 15, 30, 90, 150, and 300 mA/g. At the current density of 7.5 mA/g, the initial capacities of all the ASSLBs ranged from 90 to 130 mA h/g, which is consistent with the results shown in Figure 6a,b. However, as the current density increased, the specific

https://dx.doi.org/10.1021/acsomega.0c05942
ACS Omega 2021, 6, 6824−6835

Table 2. Specific Capacity Data of All-Solid-State In|$Li_7P_2S_8$I|$LiNi_{0.6}Co_{0.2}Mn_{0.2}O_2$ Cells Using Bare NCM622 or $NiCo_2S_4$-Coated NCM622 Cathode Materials

	calculated specific capacity (mA h/g)			
	cycle performances		C-rate performance	
material	1st cycle (15 mA/g)	last cycle (15 mA/g)	1st c-rate (7.5 mA/g)	last c-rate (7.5 mA/g)
bare NCM	86.0	41.3	121.82	73.2
0.1 wt % $NiCo_2S_4$ @ NCM	115.9	51.3	125.97	90.6
0.3 wt % $NiCo_2S_4$ @ NCM	118.0	71.5	128.7	122.4
0.5 wt % $NiCo_2S_4$ @ NCM	84.7	68.9	98.9	75.8

capacities of the ASSLBs drastically decreased. Especially, the specific capacity of bare NCM622 greatly decreased at a current density of 30 mA/g down to 5080 mA h/g. This suggests that the internal resistance of the fabricated ASSLBs device was much higher than that of the available conventional lithium-ion batteries.

In addition, at high current densities (150 and 300 mA/g), the specific capacities of all the samples were nearly zero, which indicates that the current density of 150 or 300 mA/g exhibits poor performance at room temperature. Meanwhile, the 0.3 wt% $NiCo_2S_4$-coated NCM622 cell maintained good rate characteristics, with a specific capacity of 122.4 mA h/g after high rate performances of 2 C-rate. In addition, all ASSLBs using the $NiCo_2S_4$-coated cathodes demonstrated a higher specific capacity than that of the bare NCM622 material. Generally, the side reactions at the cathode-sulfide-based electrolyte interface increased the interfacial resistance of ASSLBs by forming an undesirable interface layer. This interfacial resistance reduced the capacity and inferior rate performance of the ASSLBs. Thus, the $NiCo_2S_4$-coated NCM622 cathode exhibited a higher specific capacity and improved rate performance because of the minimal side reactions at the cathode−solid electrolyte interface. These results demonstrate the success of the proposed resonant acoustic coating of $NiCo_2S_4$ NPs on NCM 622.

After 20 cycles, the transient discharge potential profiles from the GITT experiments were elucidated to determine whether the surface area decreased, and the results are presented in Figure 8. For this measurement, all cells of $NiCo_2S_4$-coated NCM622 were chosen. The corresponding closed-circuit voltage and quasi-open-circuit voltage graphs are shown in Figure 8a,b.[29] The 0.1, 0.3, and 0.5 wt% $NiCo_2S_4$-coated NCM622 electrodes exhibited the highest surface coverage (33.2, 35.0, and 25.2%, respectively), whereas the

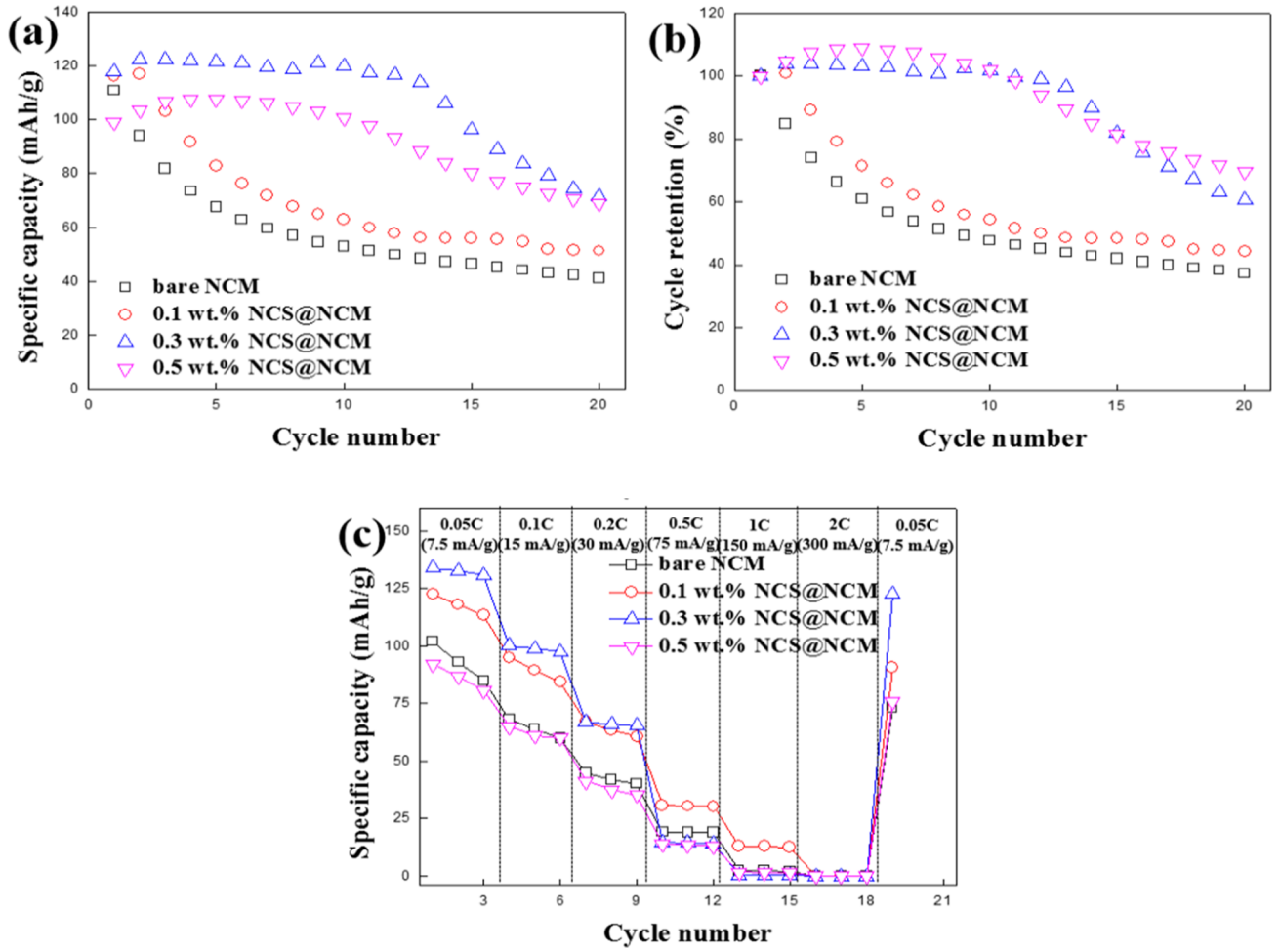

Figure 7. (a) Cycle performances of $NiCo_2S_4$-coated NCM622 at a current density of 15 mA/g (0.1 c-rate), (b) cycle retentions of $NiCo_2S_4$-coated NCM622 from the cycle performance, and (c) C-rate performances of $NiCo_2S_4$-coated NCM622 at a current density of 0.05−0.1, 0.2, 0.5, 1, 2, and 0.05 C-rate using the In|$Li_7P_2S_8$I|$LiNi_{0.6}Co_{0.2}Mn_{0.2}O_2$ cell assemblies in the range of 3.68−2.38 V.

https://dx.doi.org/10.1021/acsomega.0c05942
ACS Omega 2021, 6, 6824−6835

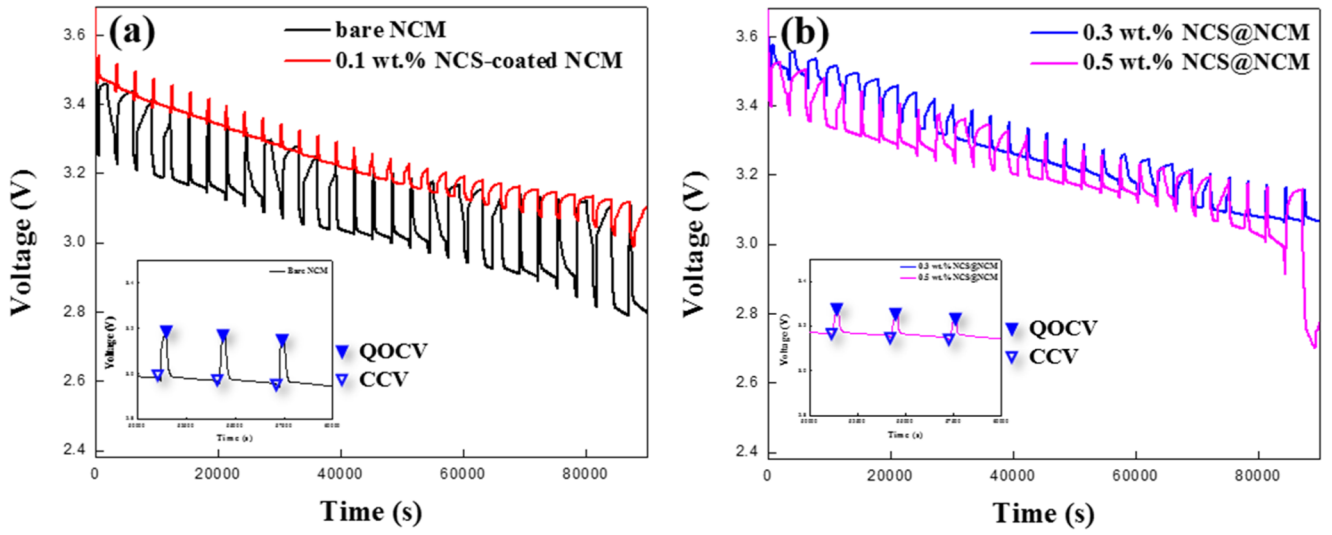

Figure 8. GITT analysis of (a) bare NCM622 with 0.1 wt% $NiCo_2S_4$-coated NCM622 and (b) 0.3 and 0.5 wt% $NiCo_2S_4$-coated NCM622 after 20 cycles using $In|Li_7P_2S_8I|LiNi_{0.6}Co_{0.2}Mn_{0.2}O_2$ cell assemblies in the potential window range of 3.68−2.38 V.

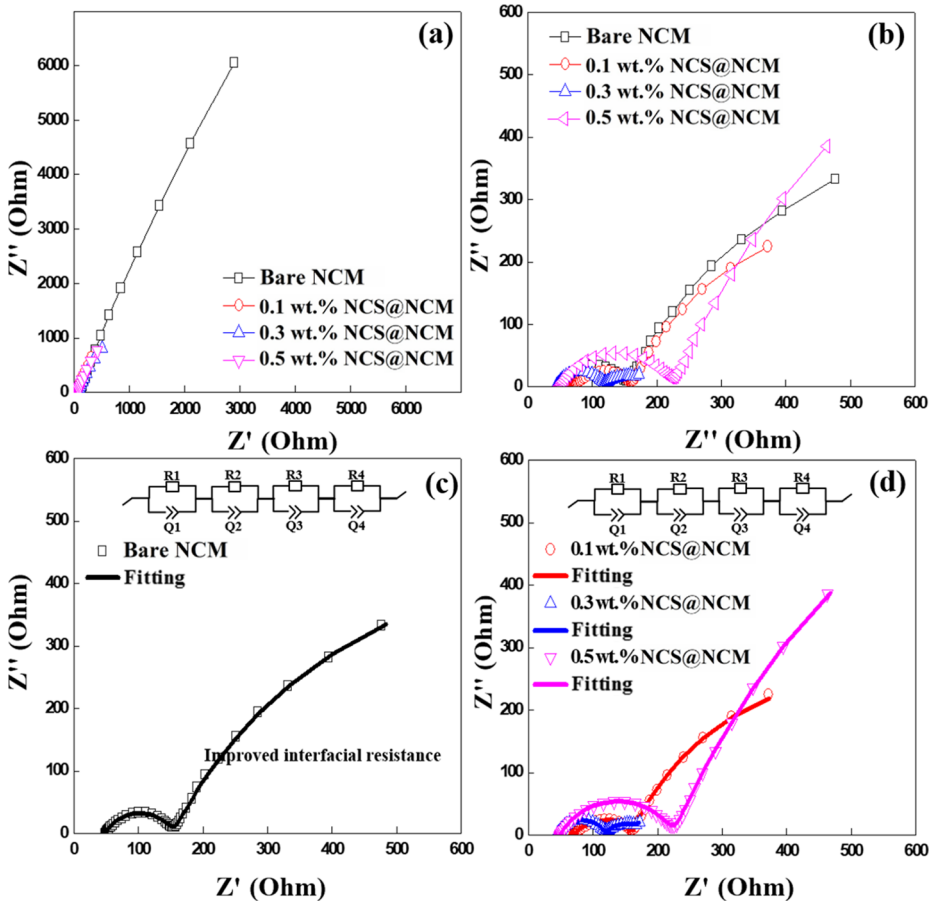

Figure 9. EIS (a) before cycling and (b) after 20 cycles and fitting simulation with raw data of (c) bare NCM622 and (d) 0.1, 0.3, and 0.5 wt% $NiCo_2S_4$-coated NCM622 composite after 20 cycles to determine the resistance differences between the sulfide-based electrolyte and the cathode material.

bare NCM622 electrode showed a contact (cathode-electrolyte) interface of 26.6%.

We tried to determine the impedance behavior of ASSLBs before (Figure 9a) and after 20 cycles (Figure 9b) using EIS between the frequency range of 1 MHz to 0.01 Hz using an SP-300 analyzer at room temperature. The obtained Nyquist spectra were fitted with the equivalent circuit and are shown in Figure 9c,d.[32−34] Figure 9c shows the Nyquist plot of the coin cell using the bare NCM622 cathode materials, and Figure 9d shows that when using 0.1, 0.3, and 0.5 wt % $NiCo_2S_4$-coated NCM622 in the $Li_{0.5}In|Li_7P_2S_8I|LiNi_{0.6}Co_{0.2}Mn_{0.2}O_2$ ASSLB system with fitting simulation. We assumed that our cells have

https://dx.doi.org/10.1021/acsomega.0c05942
ACS Omega 2021, 6, 6824−6835

Table 3. Impedance Fitting Data of All-Solid-State In|$Li_7P_2S_8I$|$LiNi_{0.6}Co_{0.2}Mn_{0.2}O_2$ Cells with Bare NCM622 and $NiCo_2S_4$-Coated NCM622 Cathode Composite[a]

	resistances (Ω) equivalent circuit: (RQ) (RQ) (RQ) (RQ)			
materials	R1	R2	R3	R4
bare NCM	106.8	1.845	1245	46.46
0.1 wt % $NiCo_2S_4$ @ NCM	71.06	37.59	721	51.76
0.3 wt % $NiCo_2S_4$ @ NCM	76.69	34.63	510.1	43.57
0.5 wt % $NiCo_2S_4$ @ NCM	176.9	365.5	1678	48.7

[a]R1: bulk original resistance of the $Li_7P_2S_8I$ solid electrolyte, R2: grain boundary resistance, including $NiCo_2S_4$ NP, R3: contact loss resistance of the cathode composite, and R4: contact loss resistance of the In foil anode.

four major interfaces, such as the anode, solid electrolyte, and cathode material. The simulated values of bare NCM622 and $NiCo_2S_4$-coated NCM are listed in Table 3.

The $NiCo_2S_4$ NPs and NCM622 cathode materials in ASSLBs have four different resistance components. The resistance values of bare NCM622 from R1 to R4 were 106.8, 1.845, 1245, and 46.46 Ω and those of 0.1 wt% $NiCo_2S_4$-coated NCM622 were 71.06, 37.59, 721, and 51.76 Ω and those of 0.3 wt% $NiCo_2S_4$-coated NCM cathode battery assembly (Figure 9d) were 76.69, 34.63, 510.1, and 43.57 Ω, respectively. R1 and R4 were similar to that of bare NCM622. R3 of 0.1 wt% $NiCo_2S_4$-coated NCM622 was slightly larger than that of 0.3 wt% $NiCo_2S_4$-coated NCM622 but smaller than that of bare NCM622. All the values of 0.3 wt% $NiCo_2S_4$-coated NCM622 were remarkably relieved, suggesting that it was the best composition. The 0.5 wt% $NiCo_2S_4$-coated NCM622 (Figure 9d) exhibited resistance fitting values for R1 to R4 of 176.9, 365.5, 1678, and 48.7 Ω, respectively. The R3 resistance showed that almost all samples exhibited poor interfacial resistance by contact loss except for the 0.5 wt% $NiCo_2S_4$-coated NCM622 battery assembly.

We identified the metal sulfide effects between the cathode and the solid electrolyte more clearly for precision research of the interfacial chemistry specified by XPS and TEM−EELS analysis to observe the inside of ASSLBs. After charge and discharge cycling (20 cycles), the side reactions and qualitative analysis of the interface were identified by XPS, and the

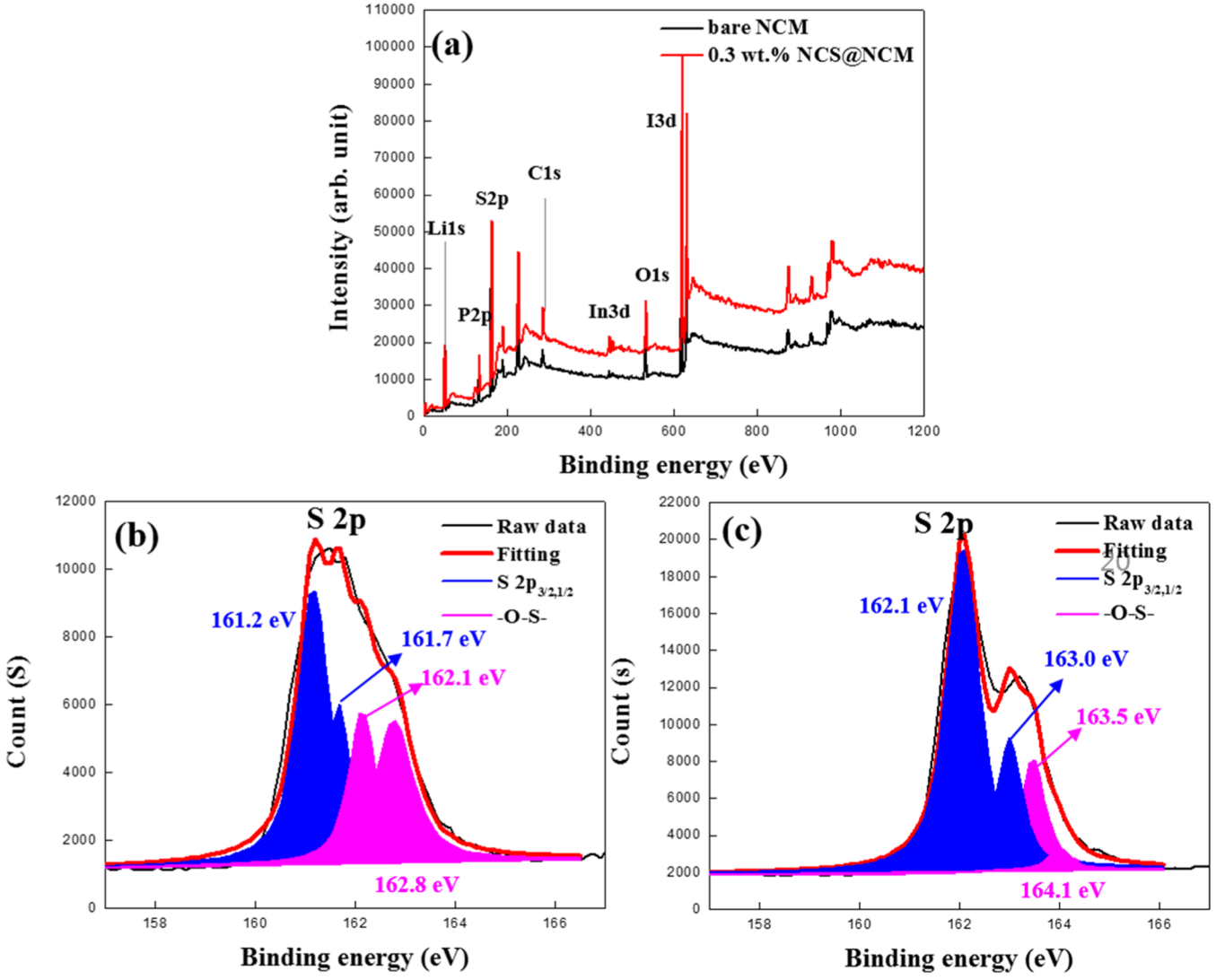

Figure 10. XPS graphs of (a) survey scan and S 2p peaks analysis of (b) bare NCM622 and (c) 0.3 wt % $NiCo_2S_4$-coated NCM622 composite after 20 cycles.

https://dx.doi.org/10.1021/acsomega.0c05942
ACS Omega 2021, 6, 6824−6835

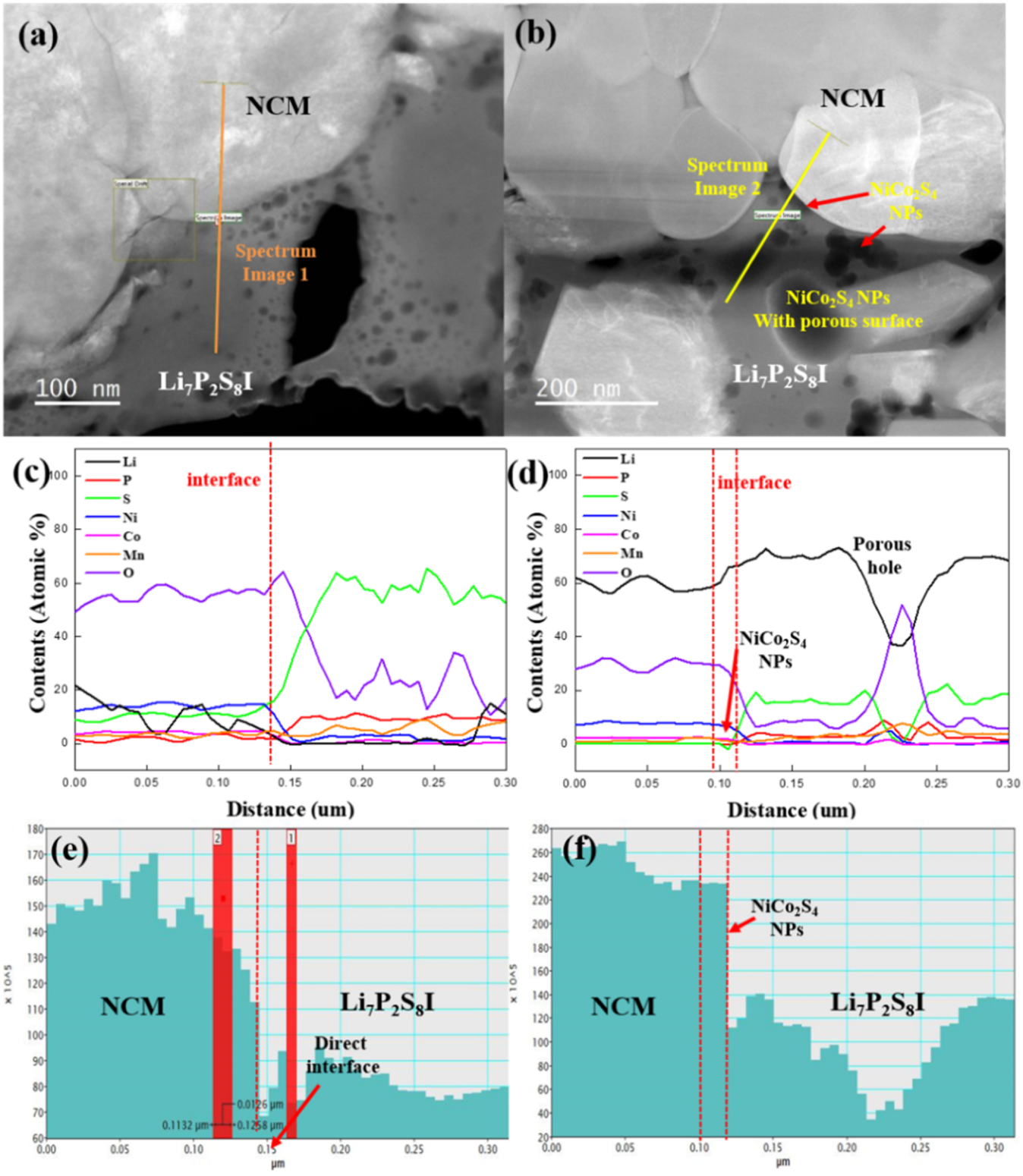

Figure 11. TEM images of (a) bare NCM622 and (b) 0.3 wt% $NiCo_2S_4$-coated NCM622 composite between NCM622 and $Li_7P_2S_8I$ solid electrolyte. Line-mapping graphs of (c) bare NCM and (d) 0.3 wt% $NiCo_2S_4$-coated NCM622 composite between NCM622 and $Li_7P_2S_8I$ solid electrolyte. Depth profiles of (e) bare NCM622 and (f) 0.3 wt% $NiCo_2S_4$-coated NCM 622 composites between NCM622 and $Li_7P_2S_8I$ solid electrolyte by EELS.

interface was visually analyzed by TEM-EELS. Figure 10 presents the XPS examination spectra of bare NCM and 0.3 wt % $NiCo_2S_4$-coated NCM622, and their examination scan spectra are shown in Figure 10a. As shown in Figure 10b, two characteristic peaks of S 2p spectrum were observed at 161.2 eV (S $2p_{1/2}$) and 161.7 eV (S $2p_{3/2}$) with the addition of −O−S− oxidation peaks of 162.1 and 162.8 eV on the bare NCM622/solid electrolyte interface. The peaks marked in pink indicate the oxidized sulfur. This peak shift suggests that a small amount of sulfur atoms from the coating materials and

https://dx.doi.org/10.1021/acsomega.0c05942
ACS Omega 2021, 6, 6824−6835

solid electrolytes propagate to NCM 622 and may react with the oxygen atoms. The S 2p peaks of the bare NCM622/solid electrolyte composite were relatively smaller than those of the coated composites.[3] NCM622 coated with 0.3 wt% $NiCo_2S_4$ showed strong S 2p (162.1, 163.0 eV, respectively) and −O−S− S 2p (163.0, 164.1 eV, respectively) peaks, possibly because of the minimal side reactions induced by the bimetal sulfide coating to satisfy the maximum compatibility of the sulfide-based solid electrolyte, as shown in Figure 10c.

Based on the XPS results, bare NCM622 and 0.3 wt% $NiCo_2S_4$-coated NCM622 were selected for TEM−EELS analysis to visualize the electrode−electrolyte interface. Overall, side reactions of S 2p can create higher binding energies by interacting with or forming side reactions with O 1s. This means that the solid electrolyte reaches a more stable state than in the previous stages, which reduces its ability in a battery, whereas $NiCo_2S_4$-coated NCM622 active materials are covered with $NiCo_2S_4$ NPs that have inert properties.

TEM imaging (Figure 11a,b) and EELS (line-mapping, Figure 11c,d) were performed to examine the cross-sectional area of the cathode composite/electrolyte interface of the bare NCM622 and 0.3 wt% $NiCo_2S_4$-coated NCM622 composite electrode-based ASSLBs after 20 cycles. This enables visual observation of the interface and interface analysis. Figure 11e,f shows the depth intensity profiles of both the images along the direction indicated by the line-mapping line of the annular dark field images (ADF-TEM). For the TEM-EELS analysis, ion beam instrument coupled with TEM was used to cut the sample from the cathode-electrolyte interface and to perform the morphology analysis. All the processes were performed in vacuum to avoid moisture. In addition, the EELS spectroscopic analysis was performed at the 0.3 wt% $NiCo_2S_4$-coated NCM622-sulfide-based $Li_7P_2S_8I$ electrolyte interface. The cross-sectional line mapping of bare NCM622 is shown in Figure 11c. Almost no lithium, and very little P and S element was detected at the interface or the solid electrolyte regions; also no P or S element was observed at the cathode part, indicating that no layer has damaged the entire NCM622 interface with significant side reaction. O element was also detected in the solid electrolyte in the ASSLBs of bare NCM622. The overall capacity at the interface decreased because of the lack of protection of these cathodes. The cross-sectional line mapping of bare 0.3 wt% $NiCo_2S_4$-coated NCM622 is shown in Figure 11d, and the complete absence of any S or P is possible evidence for the lack of side reactions at the cathode/electrolyte interface.

Figure 11e is a graph showing the depth intensity according to the distance of bare NCM622. From Figure 11e, we can determine the profile of the interface between NCM622 and electrolyte. A deep valley was formed at the interface of bare NCM622, and as the cathode site approached the electrolyte, cliffs with radical slope were formed and traces remained. This suggests that the electrolyte layer was decomposed because of direct contact and continuous side reactions, and demonstrates the need for a well-protected interface. On the other hand, as shown in Figure 11f, the $NiCo_2S_4$-coated NCM622 composite showed a protected depth image, where its surface was protected by $NiCo_2S_4$ NPs and no valley was formed. The NCM622 cathode material did not exhibit any slope adjacent to the interface, which allowed us to confirm that the chemistry at the cathode interface plays a critical role in capacity maintenance.

Commonly, cathode composites sampled by gallium ions are more damaged on the electrolyte side than on the cathode, resulting in a deeper form which is much more damaged by the ion beam because the solid electrolyte is not a harder crystallite than the cathode. Therefore, the 0.3 wt% $NiCo_2S_4$-coated NCM622 composite electrode exhibited reduced side reactions during the charge−discharge cycle, as further confirmed by the XPS analysis, as shown in Figure 10. This resulted in a relatively highly protected interface by applying the sulfide-based coating concept, compared to that of the composite electrode using bare NCM622.

4. CONCLUSIONS

$NiCo_2S_4$ NPs were introduced as a coating agent because of their stability and excellent protective effect as a coating material. NCM622 with a coating of $NiCo_2S_4$ NPs exhibited increased battery capacity compared to that of bare NCM622. Composite electrodes of the ASSLBs using 0.3 wt% $NiCo_2S_4$-coated NCM622 showed a high specific capacity with a high capacity retention of up to 60.6 and a high contact area of 35.0%, compared to that using bare NCM622. XPS analysis confirmed the reduced side reaction between the NCM622 cathode and the electrolyte. However, $NiCo_2S_4$-coated NCM622 showed highly intense S $2p_{3/2}$ and S $2p_{1/2}$ peaks, which suggested a lower side reaction or interaction as a lithium ion scavenger compared to bare NCM622. TEM−EELS analysis confirmed the successful coating of the $NiCo_2S_4$ NPs and the reduced movement of P and S elements into the cathode composite region during cycling by blocking/reducing the side reaction or interaction through direct contact. These results indicate that $NiCo_2S_4$ coating using the thermal decomposition with the resonant acoustic coating technique can minimize the side reaction between the cathode and sulfide-based solid electrolyte, thus improving the capacity of ASSLBs. Thus, we concluded that the $NiCo_2S_4$ NPs coating provided improved specific capacity and reduced interfacial resistance than bare NCM622.

AUTHOR INFORMATION

Corresponding Author

Kwang-Sun Ryu − *Department of Chemistry, University of Ulsan, Ulsan 44776, Republic of Korea;* orcid.org/0000-0002-8758-0495; Email: ryuks@ulsan.ac.kr

Authors

Young-Jin Kim − *Department of Chemistry, University of Ulsan, Ulsan 44776, Republic of Korea*

Rajesh Rajagopal − *Department of Chemistry, University of Ulsan, Ulsan 44776, Republic of Korea*

Sung Kang − *Research Institute of Industrial Science & Technology, Pohang 790-330, Republic of Korea*

Complete contact information is available at: https://pubs.acs.org/10.1021/acsomega.0c05942

Notes

The authors declare no competing financial interest.

ACKNOWLEDGMENTS

This research was supported by a grant (2018R1D1A3B07050296) of the Basic Science Research Program through the National Research Foundation (NRF) funded by the Ministry of Education, Republic of Korea.

https://dx.doi.org/10.1021/acsomega.0c05942
ACS Omega 2021, 6, 6824−6835

REFERENCES

(1) Wu, Z.; Xie, Z.; Yoshida, A.; Wang, Z.; Hao, X.; Abudula, A.; et al. Utmost limits of various solid electrolytes in all-solid-state lithium batteries: A critical review. *Renew. Sustain. Energy Rev.* **2019**, *109*, 367−385.

(2) Zheng, F.; Kotobuki, M.; Song, S.; Lai, M. O.; Lu, L. Review on solid electrolytes for all-solid-state lithium-ion batteries. *J. Power Sources* **2018**, *389*, 198−213.

(3) Lee, H.; Oh, P.; Kim, J.; Cha, H.; Chae, S.; Lee, S.; et al. Advances and Prospects of Sulfide All-Solid-State Lithium Batteries via One-to-One Comparison with Conventional Liquid Lithium Ion Batteries. *Adv. Mater.* **2019**, *31*, 1900376.

(4) Kamaya, N.; Homma, K.; Yamakawa, Y.; Hirayama, M.; Kanno, R.; Yonemura, M.; et al. A lithium superionic conductor. *Nat. Mater.* **2011**, *10*, 682−686.

(5) Kato, Y.; Hori, S.; Saito, T.; Suzuki, K.; Hirayama, M.; Mitsui, A.; et al. High-power all-solid-state batteries using sulfide superionic conductors. *Nat. Energy* **2016**, *1*, 1−7.

(6) Kwak, H. W.; Park, Y. J. Cathode coating using $LiInO_2$ -LiI composite for stable sulfide-based all-solid-state batteries. *Sci. Rep.* **2019**, *9*, 8099.

(7) Hu, G.; Tao, Y.; Lu, Y.; Fan, J.; Li, L.; Xia, J.; et al. Enhanced Electrochemical Properties of $LiNi_{0.8}Co_{0.1}Mn_{0.1}O_2$ Cathode Materials Modified with Lithium-Ion Conductive Coating $LiNbO_3$. *ChemElectroChem* **2019**, *6*, 4773−4780.

(8) Fan, X.; Ji, X.; Han, F.; Yue, J.; Chen, J.; Chen, L.; et al. Fluorinated solid electrolyte interphase enables highly reversible solid-state Li metal battery. *Sci. Adv.* **2018**, *4*, No. eaau9245.

(9) Hu, G.; Qi, X.; Hu, K.; Lai, X.; Zhang, X.; Du, K.; et al. A facile cathode design with a $LiNi_{0.6}Co_{0.2}Mn_{0.2}O_2$ core and an AlF3-activated $Li_{1.2}Ni_{0.2}Mn_{0.6}O_2$ shell for Li-ion batteries. *Electrochim. Acta* **2018**, *265*, 391−399.

(10) Sakuda, A.; Hayashi, A.; Tatsumisago, M. Interfacial Observation between $LiCoO_2$ Electrode and Li2S−P2S5 Solid Electrolytes of All-Solid-State Lithium Secondary Batteries Using Transmission Electron Microscopy. *Chem. Mater.* **2010**, *22*, 949−956.

(11) Haruyama, J.; Sodeyama, K.; Han, L.; Takada, K.; Tateyama, Y. Space−Charge Layer Effect at Interface between Oxide Cathode and Sulfide Electrolyte in All-Solid-State Lithium-Ion Battery. *Chem. Mater.* **2014**, *26*, 4248−4255.

(12) Takada, K.; Ohta, N.; Zhang, L.; Fukuda, K.; Sakaguchi, I.; Ma, R.; et al. Interfacial modification for high-power solid-state lithium batteries. *Solid State Ionics* **2008**, *179*, 1333−1337.

(13) Ohta, N.; Takada, K.; Sakaguchi, I.; Zhang, L.; Ma, R.; Fukuda, K.; et al. $LiNbO_3$-coated $LiCoO_2$ as cathode material for all solid-state lithium secondary batteries. *Electrochem. Commun.* **2007**, *9*, 1486−1490.

(14) Kim, J.; Kim, M.; Noh, S.; Lee, G.; Shin, D. Enhanced electrochemical performance of surface modified $LiCoO_2$ for all-solid-state lithium batteries. *Ceram. Int.* **2016**, *42*, 2140−2146.

(15) Lee, J. W.; Park, Y. J. Enhanced Cathode/Sulfide Electrolyte Interface Stability Using an Li_2ZrO_3 Coating for All-Solid-State Batteries. *J. Electrochem. Sci. Technol.* **2018**, *9*, 176−183.

(16) Okada, K.; Machida, N.; Naito, M.; Shigematsu, T.; Ito, S.; Fujiki, S.; et al. Preparation and electrochemical properties of $LiAlO_2$-coated $Li(Ni_{1/3}Mn_{1/3}Co_{1/3})O_2$ for all-solid-state batteries. *Solid State Ionics* **2014**, *255*, 120−127.

(17) Sakuda, A.; Nakamoto, N.; Kitaura, H.; Hayashi, A.; Tadanaga, K.; Tatsumisago, M. All-solid-state lithium secondary batteries with metal-sulfide-coated $LiCoO_2$ prepared by thermal decomposition of dithiocarbamato complexes. *J. Mater. Chem.* **2012**, *22*, 15247−15254.

(18) Xiao, Y.; Su, D.; Wang, X.; Zhou, L.; Wu, S.; Li, F.; et al. In suit growth of ultradispersed $NiCo_2S_4$ nanoparticles on graphene for asymmetric supercapacitors. *Electrochim. Acta* **2015**, *176*, 44−50.

(19) Zhu, Y.; Wu, Z.; Jing, M.; Yang, X.; Song, W.; Ji, X. Mesoporous $NiCo_2S_4$ nanoparticles as high-performance electrode materials for supercapacitors. *J. Power Sources* **2015**, *273*, 584−590.

(20) Vanarase, A.; Osorio, J.; Muzzio, F.; Coguill, S.; Lucon, P. Resonant acoustic ® mixing; uniform distribution of minor materials during powder mixing. *JANNAF 36th Propellant and Explosives Development and Characterization Joint*, 2010.

(21) Anderson, S. R.; am Ende, D. J.; Salan, J. S.; Samuels, P. Preparation of an Energetic-Energetic Cocrystal using Resonant Acoustic Mixing. *Propellants, Explos., Pyrotech.* **2014**, *39*, 637−640.

(22) am Ende, D. J.; Anderson, S. R.; Salan, J. S. Development and Scale-Up of Cocrystals Using Resonant Acoustic Mixing. *Org. Process Res. Dev.* **2014**, *18*, 331−341.

(23) Osorio, J. G.; Muzzio, F. J. Evaluation of resonant acoustic mixing performance. *Powder Technol.* **2015**, *278*, 46−56.

(24) Kim, Y.-J.; Rajagopal, R.; Kang, S.; Ryu, K.-S. Novel dry deposition of $LiNbO_3$ or Li_2ZrO_3 on $LiNi_{0.6}Co_{0.2}Mn_{0.2}O_2$ for high performance all-solid-state lithium batteries. *Chem. Eng. J.* **2020**, *386*, 123975.

(25) Sakuda, A.; Hayashi, A.; Tatsumisago, M. Sulfide Solid Electrolyte with Favorable Mechanical Property for All-Solid-State Lithium Battery. *Sci. Rep.* **2013**, *3*, 2261.

(26) Choi, S.-J.; Lee, S.-H.; Ha, Y.-C.; Yu, J.-H.; Doh, C.-H.; Lee, Y.; et al. Synthesis and Electrochemical Characterization of a Glass-Ceramic $Li_7P_2S_8I$ Solid Electrolyte for All-Solid-State Li-Ion Batteries. *J. Electrochem. Soc.* **2018**, *165*, A957.

(27) Yamada, T.; Ito, S.; Omoda, R.; Watanabe, T.; Aihara, Y.; Agostini, M.; et al. All Solid-State Lithium−Sulfur Battery Using a Glass-Type P_2S_5−Li_2S Electrolyte: Benefits on Anode Kinetics. *J. Electrochem. Soc.* **2015**, *162*, A646.

(28) Wang, S.; Xu, H.; Li, W.; Dolocan, A.; Manthiram, A. Interfacial Chemistry in Solid-State Batteries: Formation of Interphase and Its Consequences. *J. Am. Chem. Soc.* **2018**, *140*, 250−257.

(29) Nam, Y. J.; Oh, D. Y.; Jung, S. H.; Jung, Y. S. Toward practical all-solid-state lithium-ion batteries with high energy density and safety: Comparative study for electrodes fabricated by dry- and slurry-mixing processes. *J. Power Sources* **2018**, *375*, 93−101.

(30) Huang, Y.; Jin, F.-M.; Chen, F.-J.; Chen, L. Improved cycle stability and high-rate capability of Li_3VO_4-coated Li-$[Ni_{0.5}Co_{0.2}Mn_{0.3}]O_2$ cathode material under different voltages. *J. Power Sources* **2014**, *256*, 1−7.

(31) Tan, S.; Wang, L.; Bian, L.; Xu, J.; Ren, W.; Hu, P.; et al. Highly enhanced low temperature discharge capacity of $LiNi_{1/3}Co_{1/3}Mn_{1/3}O_2$ with lithium boron oxide glass modification. *J. Power Sources* **2015**, *277*, 139−146.

(32) Choi, S.-J.; Choi, S.-H.; Bui, A. D.; Lee, Y.-J.; Lee, S.-M.; Shin, H.-C.; et al. LiI-Doped Sulfide Solid Electrolyte: Enabling a High-Capacity Slurry-Cast Electrode by Low-Temperature Post-Sintering for Practical All-Solid-State Lithium Batteries. *ACS Appl. Mater. Interfaces* **2018**, *10*, 31404−31412.

(33) Ito, S.; Unemoto, A.; Ogawa, H.; Tomai, T.; Honma, I. Application of quasi-solid-state silica nanoparticles−ionic liquid composite electrolytes to all-solid-state lithium secondary battery. *J. Power Sources* **2012**, *208*, 271−275.

(34) Koerver, R.; Aygün, I.; Leichtweiß, T.; Dietrich, C.; Zhang, W.; Binder, J. O.; et al. Capacity Fade in Solid-State Batteries: Interphase Formation and Chemomechanical Processes in Nickel-Rich Layered Oxide Cathodes and Lithium Thiophosphate Solid Electrolytes. *Chem. Mater.* **2017**, *29*, 5574−5582.

https://dx.doi.org/10.1021/acsomega.0c05942
ACS Omega 2021, 6, 6824−6835